HHS Public Access

Author manuscript

Curr Biol. Author manuscript; available in PMC 2023 July 11.

Published in final edited form as:

Curr Biol. 2022 July 11; 32(13): 2962–2971.e4. doi:10.1016/j.cub.2022.05.009.

Cross-species incompatibility between a DNA satellite and the Drosophila Spartan homolog poisons germline genome integrity

Cara L. Brand,

Mia T. Levine*

Department of Biology and Epigenetics Institute, University of Pennsylvania, 433 S. University Avenue, Philadelphia, PA 19104.

SUMMARY

Satellite DNA spans megabases of eukaryotic sequence and evolves rapidly.[1–6] Paradoxically, satellite-rich genomic regions mediate strictly conserved, essential processes like chromosome segregation and nuclear structure.[7–10] A leading resolution to this paradox posits that satellite DNA and satellite-associated chromosomal proteins coevolve to preserve these essential functions.[11] We experimentally test this model of intra-genomic coevolution by conducting the first evolution-guided manipulation of both chromosomal protein and DNA satellite. The *359bp* satellite spans an 11Mb array in *Drosophila melanogaster* that is absent from its sister species, *Drosophila simulans*.[12–14] This species-specific DNA satellite colocalizes with the adaptively evolving, ovary-enriched protein, Maternal Haploid (MH)–the *Drosophila* homolog of Spartan.[15] To determine if MH and *359bp* coevolve, we swapped the *D. simulans* version of MH ("MH[sim]") into *D. melanogaster*. MH[sim] triggers ovarian cell death, reduced ovary size, and loss of mature eggs. Surprisingly, the *D. melanogaster mh* null mutant has no such ovary phenotypes[15], suggesting that MH[sim] is toxic in a *D. melanogaster* background. Using both cell biology and genetics, we discovered that MH[sim] poisons oogenesis through a DNA damage pathway. Remarkably, deleting the *D. melanogaster*-specific *359bp* satellite array completely restores *mh[sim]* germline genome integrity and fertility, consistent with a history of coevolution between these two fast-evolving loci. Germline genome integrity and fertility are also restored by overexpressing Topoisomerase II (Top2), suggesting that MH[sim] interferes with Top2-mediated processing of *359bp*. The observed *359bp*-MH[sim] cross-species incompatibility supports a model under which seemingly inert repetitive DNA and essential chromosomal proteins must coevolve to preserve germline genome integrity.

*Lead Contact: Dr. Mia Levine, University of Pennsylvania, 433 S. University Avenue, Philadelphia, PA 19104. p: 215-573-9709 m.levine@sas.upenn.edu. Twitter handle: @levine_lab.

AUTHOR CONTRIBUTIONS

Conceptualization, M.T.L and C.L.B.; Methodology, M.T.L and C.L.B.; Investigation, M.T.L and C.L.B; Writing M.T.L and C.L.B; Funding Acquisition, M.T.L and C.L.B.

DECLARATION OF INTERESTS

The authors declare no competing interests.

Graphical Abstract

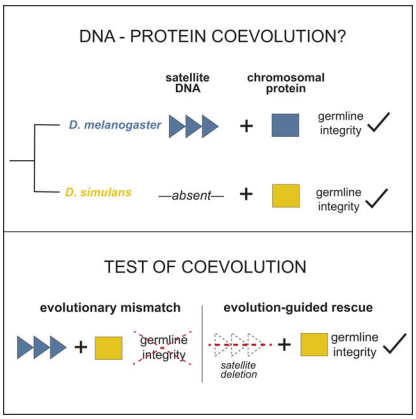

eTOC BLURB

Rapid evolution of DNA repeats is thought to trigger rapid evolution of proteins that package and process DNA repeats. Brand and Levine genetically manipulate both protein and DNA satellite to define the molecular players engaged in this intra-genomic coevolution and to reveal the chromosome biology preserved by this coevolution.

Keywords

DNA satellite; coevolution; maternal haploid; *359bp* ; Spartan; Topoisomerase II

RESULTS AND DISCUSSION

DNA satellite-enriched genomic regions evolve rapidly and yet support strictly conserved nuclear functions, including chromosome segregation, chromosome tethering, and telomere integrity.[1–10] A classic resolution to this paradox posits that DNA satellite-associated proteins evolve adaptively to mitigate deleterious proliferation of DNA satellite sequence variants.[11] Repeated bouts of DNA satellite evolution and chromosomal protein adaptation result in exquisitely coevolved satellites and satellite-associated proteins. This model of coevolution predicts pervasive incompatibilities between satellite DNA and chromosomal proteins from closely related species: adaptively evolving chromosomal proteins from one species should fail to package or process DNA satellites from another.[11,16,17]

Evidence for this coevolution model has emerged from engineering “evolutionary mismatches” between the adaptively evolving chromosomal protein(s) of one species and the DNA satellite landscape of a close relative. Under one approach, a diverged chromosomal protein is introduced into a closely related species, generating an evolutionary mismatch between the manipulated protein and one or more DNA satellites.[17–20] Consistent with disrupted DNA satellite:chromosomal protein coevolution, the naïve protein typically perturbs a satellite-mediated function, such as chromosome segregation or nuclear organization.[17,19,20] In these cases, however, the incompatible DNA satellites are unknown. A second approach crosses sister species to generate evolutionary mismatches between

chromosomal proteins and DNA satellites in hybrid progeny. Consistent with disrupted DNA satellite:chromosomal protein coevolution, interspecies hybrid inviability has been linked to satellite-rich genomic loci.[21,22] In these systems, however, the incompatible chromosomal proteins are unknown. To date, there are no cases of experimental identification of both chromosomal protein and satellite engaged in coevolution.

To experimentally probe *both sides* of the coevolution model, we searched for a rapidly evolving DNA satellite associated with an adaptively evolving chromosomal protein. In *Drosophila melanogaster*, the *359bp* satellite spans an 11Mb array at the base of the *X* chromosome.[12,13] Close relatives of *D. melanogaster*, including *D. simulans* and *D. erecta*, lack this *X*-linked satellite array.[14] Instead, these species have shorter arrays of "*359bp*-like" sequence dispersed throughout heterochromatin and euchromatin.[23–25] Such extreme lineage-restriction to *D. melanogaster* makes this DNA satellite array an ideal locus for testing the coevolution model.

On the protein side, we identified from the literature Maternal Haploid (MH), an ovary-enriched protein that is maternally provisioned to the embryo, colocalizes with the *359bp* satellite, and supports genome integrity.[15,26,27] Embryos of *mh* null mothers suffer paternal chromosome mis-segregation at the very first mitosis, suggesting that the maternally-provisioned MH prepares the otherwise inert, sperm-deposited paternal chromosomes for participation in embryonic mitosis.[15,26] Most of these embryos arrest around the first mitotic division. A smaller fraction develop beyond the first division, cycling only the "maternal haploid" complement of chromosomes until arrest prior to hatching.[15,26,28] The mechanism by which MH primes paternal chromosomes for embryonic mitosis is not known; however, the human homolog of MH, called Spartan, is a well-characterized protease.[29–31] Spartan resolves DNA-protein crosslinks that block DNA replication, chromatin remodeling, and DNA repair.[30,32] In Drosophila, MH may play an analogous role in DNA-protein crosslink resolution during paternal chromosome processing.

If the *D. melanogaster*-specific *359bp* proliferation triggered *mh* to innovate, we should detect evidence of positive selection at *mh* between *D. melanogaster* and *D. simulans*. To determine if *mh* evolves adaptively, we conducted a McDonald-Kreitman test[33] using polymorphism within *D. melanogaster* and *D. simulans* populations and divergence between *D. melanogaster* and *D. simulans* (2.5 million years diverged[34]). This comparison revealed an excess of nonsynonymous fixations, consistent with a history of adaptive evolution (Figure 1A, Table S1). The dynamic evolution of the *359bp* satellite and adaptive evolution of a *359bp*-associated protein, MH, raises the possibility that *mh* recurrently evolves to preserve a biological function compromised by *359bp* satellite proliferation.

To test the possibility of MH:*359bp* coevolution, we first conducted an evolution-guided manipulation of *mh* to generate an "evolutionary mismatch" between protein and satellite. We used CRISPR/Cas9 to integrate into the native *mh* locus of *D. melanogaster* either a 3xFLAG-tagged *mh* coding sequence from *D. melanogaster* (our control fly, "*mh[mel]*") or a 3xFLAG-tagged *mh* coding sequence from *D. simulans* (our experimental fly, "*mh[sim]*", Figure 1B). Both the *D. melanogaster* and the *D. simulans* coding sequences were codon-

optimized for *D. melanogaster*. We observed equivalent expression of the two transgenes (Figure S1A).

The *mh* null mutant phenotype in the early embryo motivated our prediction that an evolutionary mismatch between the *D. simulans mh* and the *D. melanogaster 359bp X*-linked array would disrupt the first mitotic division. We reasoned that in its native *D. simulans* background, MH[sim] efficiently processes all *D. simulans* paternal chromosomes. In a *D. melanogaster* background, we predicted that MH[sim] would process most *D. melanogaster* chromosomes but fail to recognize and process the *D. melanogaster*-specific *359bp* array, triggering mis-segregation of the paternal *X*-chromosome. This defect would result in reduced female fertility and a dearth of female progeny. We discovered that *mh[sim]* females produced significantly fewer progeny than control *mh[mel]* females (Figure 1C); however, contrary to our prediction, the progeny sex ratio did not deviate from 50/50 (Figure S1B). These data suggest that paternal *359bp* is *not* uniquely vulnerable to the presence of MH[sim] during the first mitotic division. Consistent with this inference, we observed that *mh[sim]* completely rescues the first mitotic division: embryos from *mh[mel]* and *mh[sim]* mothers show equivalent, normal distributions of embryonic stages from a 70-minute collection (Figure 1D). In contrast, embryos produced by *mh* null mothers typically arrest during the first division (Figure 1D). Moreover, we observed no evidence of elevated maternal haploid embryos from *mh[sim]* mothers (Figure S1C). These data suggest that *mh[sim]* does not phenocopy the *mh* null early embryonic phenotype.

To uncover an alternative source of the *mh[sim]* fertility defect, we looked at the developmental stage just before the first embryonic mitosis: oogenesis. Although *mh* is highly expressed during oogenesis, previous reports suggested that *mh* null mutation alone yields no ovary phenotype.[15,26] We similarly detected no difference in ovary size or mature egg number of *mh* null mothers compared to heterozygous controls (Figure S1D,E). In contrast, *mh[sim]* ovaries are significantly smaller than *mh[mel]* ovaries and are depleted of the most mature egg stages (Figure 1E,F). This unexpected *mh[sim]* ovary phenotype, combined with the complete rescue of the first embryonic division by *mh[sim]*, suggests that *mh[sim]* does not behave as a loss-of-function allele. Instead, MH[sim] might be toxic.

To explore the possibility that MH[sim] is toxic, we first asked if MH[sim] localizes aberrantly in the ovary. We visualized MH[mel] and MH[sim] by staining ovaries with anti-FLAG. We discovered that MH[mel] localized primarily in the earliest stages of oogenesis (the germarium, Figure 2A,B). MH[sim] localized in these cell types as well as on the nurse cell nuclei of later stage egg chambers (Figure 2A,B). The aberrant persistence of MH[sim] during oogenesis, combined with compromised *mh[sim]* ovary development, raised the possibility that MH mislocalization alone might be toxic. To test this hypothesis, we used the UAS/GAL4 system to overexpress MH[mel] in the female germline (driver nos-Gal4-VP16). In ovaries overexpressing MH[mel], we indeed observed elevated levels and aberrant localization of the protein in later stage egg chambers (Figure S2A). Nevertheless, these females gave rise to abundant progeny (Figure S2B), suggesting that mislocalization alone cannot explain the compromised ovary development of *mh[sim]* females. In contrast, overexpression of MH[sim] resulted in an absence of mature eggs (Figures S2C,D). Consequently, these females were completely sterile (Figure S2B). These

data suggest that MH[sim] – which functions normally in its native *D. simulans* genome – is toxic to oogenesis in *D. melanogaster*. This toxicity appears to be dose-dependent: heterozygous *mh[mel]/mh[sim]* females give rise to progeny counts similar to *mh[mel]* homozygotes (Figure S2E).

To study the cell biological basis of this block to oogenesis, we turned back to ovaries of females expressing the CRISPR-introduced *mh[mel]* or *mh[sim]* transgene under the native promoter (Figure 1B). We observed an excess of hyper-condensed nuclei in *mh[sim]* ovaries, consistent with elevated cell death (Figure 2C[35,36]). A classic trigger of cell death is the accumulation of DNA damage.[37] To visualize DNA damage, we stained *mh[mel]* and *mh[sim]* ovaries for the double-strand break marker, γH2Av.[38,39] We observed elevated DNA damage signaling in *mh[sim]* ovaries (Figure 2D, S3A). This phenotype further distinguishes *mh[sim]* from *mh* null ovaries – *mh* null ovaries show no evidence of elevated DNA damage (Figure S3B). To address the hypothesis that MH[sim] compromises oogenesis through a DNA repair pathway, we combined *mh[sim]* with a null mutation in a DNA damage checkpoint gene. The gene, *Chk2* (also known as *mnk*), normally blocks egg production in the presence of DNA damage.[40,41] $Chk2^{-/-}$ ovaries bypass this checkpoint, allowing a female to make mature but damaged eggs in the presence of elevated DNA damage. We discovered that $Chk2^{-/-}$ restores *mh[sim]* ovaries to *mh[mel]*-like ovary size and *mh[mel]*-like egg production (Figure 2E,F). However, the *mh[sim]*;$Chk2^{-/-}$ females are sterile while *mh[mel]*;$Chk^{-/-}$ females retain fertility (Figure S3C). These data suggest that MH[sim] compromises oogenesis by triggering DNA damage.

Applying these phenotypic data to the coevolution model, we hypothesized that MH[sim]-induced DNA damage depends on the 11Mb array of *359bp* satellite in *D. melanogaster*. Under this model, MH[sim]-specific residues are incompatible with *359bp*. Removing *359bp* should restore germline genome integrity and fertility of *mh[sim]* females. To directly test this prediction, we took advantage of a fly strain that lacks the 11Mb array of *X*-linked *359bp* satellite (Figure 3A[42]). We recombined this *359bp* deletion, called *Zygotic hybrid rescue* (*Zhr*) onto both the *mh[mel]* and the *mh[sim] X* chromosomes (Figure 3B). If MH[sim]-induced toxicity depends on the presence of the *359bp* expansion, *mh[sim],Zhr* females should have minimal DNA damage and recover fertility. Remarkably, the *359bp* deletion completely restores the DNA damage marker, γH2Av, to wildtype (low) levels (Figure 3C). Consistent with restored germline genome integrity of *mh[sim]* females, we observed no difference in ovary size and no difference in egg production between *mh[mel]* and *mh[sim]* females that lack *359bp* (Figure 3D,E). Finally, the *359bp* deletion completely restores *mh[sim]* fertility to *mh[mel]* levels (Figure 3F). These data reveal that MH[sim] toxicity depends on *359bp*, consistent with a history of coevolution between these two fast-evolving components of the Drosophila genome.

The observed *359bp*-dependent toxicity, rather than loss-of-function, suggests that MH[sim] may *interfere* with the preservation of *359bp* integrity. To define a molecular basis for this interference, we used well-characterized MH homologs as guides. The MH homologs in worm (DVC-1) and human (Spartan) use the conserved Spartan metalloprotease domain to repair DNA-protein crosslinks. A major substrate of Spartan/DVC-1-directed repair is Topoisomerase II (Top2).[31,43,44] Top2 transiently crosslinks with DNA as it resolves

torsional stress and DNA entanglements. Spartan/DVC-1 degrades Top2 when these crosslinks become irreversible and threaten various DNA transactions, including DNA replication, chromatin remodeling, and repair.[45–47] In *D. melanogaster*, Top2 specifically cleaves *359bp*[48] and resolves DNA entanglements involving *359bp* during female meiosis.[49] Moreover, *Top2* and *mh* genetically interact in the ovary and colocalize in the embryo.[15] We hypothesized that MH[sim] interferes with Top2 resolution of *359bp* entanglements during oogenesis.

This interference model predicts that Top2 is limiting in the presence of MH[sim]. To test this prediction, we reduced Top2 using a heterozygous loss-of-function mutant and overexpressed Top2 in the ovary using the UAS/GAL4 system in an *mh[mel]* or *mh[sim]* background. Reduction of Top2 exacerbates *mh[sim]*-dependent subfertility (Figure 4A) while Top2 overexpression in the ovary completely rescues *mh[sim]* fertility (Figure 4B). The rescued *mh[sim]* ovaries also showed restored genome integrity (Figure 4C). Excess Top2 appears to mitigate MH[sim] interference. Combined with the literature on DNA-Top2 crosslink resolution by MH homologs DVC-1 and Spartan, these data raise the possibility that MH[sim] over-actively clears Top2:*359bp* associations that otherwise resolve *359bp* entanglements in the female germline. Persistent DNA entanglements would trigger the observed DNA damage that blocks oogenesis progression (Figure 4D). Intriguingly, a sliding window analysis of *D. melanogaster*-specific *mh* evolution revealed a striking enrichment of elevated dN/dS in multiple regions of the C-terminus (Figure S4A). The C-terminus of Spartan mediates both its recruitment to chromatin[50,51] and its self-cleavage activity.[30,52] Lineage-specific evolution of either recruitment to chromatin or autoregulation could modulate MH activity at *359bp*.

Our model is motivated in part by the observation that repeat-rich genomic regions, and especially the 11Mb array of *359bp*, is uniquely vulnerable to DNA entanglements.[21,49,53] If *359bp* is so deleterious, how could it have proliferated? DNA satellites can behave selfishly, gaining a transmission advantage from one generation to the next.[54,55] We suspect that such non-Mendelian segregation led to *359bp* proliferation, triggering MH to evolve adaptively along the *D. melanogaster* lineage (Figure 4E). We lack sufficient power to detect such lineage-specific adaptive evolution under a McDonald-Kreitman test framework (Table S1); however, a sliding window dN/dS analysis between the reconstructed ancestral *mh* sequence and either *mh[mel]* or *mh[sim]* revealed a highly significant enrichment of codons with elevated dN/dS along the *D. melanogaster* branch (FET, $p < 0.0001$, Figure S4A, Table S2). This finding is consistent with *359bp* proliferation leading to positive selection on *mh*. However, we cannot formally rule out the possibility that a selection pressure distinct from *359bp* proliferation shaped *mh[mel]* adaptive evolution. Under this alternative model, the *D. melanogaster* version of MH evolved first, releasing constraint on *359bp* copy number. Most likely, both selection and loss of constraint operate cyclically.

Regardless of the force(s) that promoted *359bp* proliferation, the *359bp*:MH system offers two important elaborations of the classic model of intra-genomic coevolution.[11,56–58] This canonical model posits that chromosomal proteins evolve adaptively to recognize and process novel satellite repeat variants. Under this model, the mismatched *mh[sim]* allele should fail to perform an *mh* function; that is, act as a loss-of-function allele. Instead,

we demonstrate that *mh[sim]* is toxic, suggesting that *mh[mel]* evolved adaptively to *avoid interfering* with *359bp* processing. The canonical coevolution model also envisioned coevolution sculpting specifically a DNA-protein interface. However, MH lacks a sequence-specific DNA binding domain[26,51], rejecting the possibility that MH evolves to reduce *359bp* sequence recognition. MH adaptive evolution instead likely tracks Top2, and more specifically, Top2-*359bp* crosslinks. This speculative model suggests that *359bp*:MH coevolution is indirect: MH tracks Top2 evolution and Top2 evolution tracks *359bp* evolution. Under this model, Top2 should evolve adaptively. To test this possibility, we implemented a McDonald-Kreitman test on Top2 alleles from *D. melanogaster* and *D. simulans*. We discovered that Top2 indeed evolves adaptively between these sister species (Figure S4B). Future research will test this model of *359bp*-triggered evolution of the protein:protein interaction interface between MH and Top2.

359bp-mediated toxicity to oogenesis highlights the catastrophic functional consequences of DNA satellite evolution. Importantly, *359bp*-mediated toxicity is also apparent in *D. melanogaster-D. simulans* hybrid embryos: a distinct, unmapped gene on *D. simulans* chromosome *2*[59–62] interacts deleteriously with *359bp* to cause embryonic chromosome mis-segregation, genome instability, and lethality.[21,42,63] This interspecies hybrid dysfunction in the embryo, together with the *359bp:mh[sim]* toxicity in the ovary reported here, suggests that recurrent bouts of coevolution not only shape essential genome functions within species but also can trigger hybrid incompatibilities between species.

STAR METHODS

(see separate Word document for STAR METHODS Table)

RESOURCE AVAILABILITY

Lead contact—Further information and requests for resources and reagents should be directed to and will be fulfilled by the lead contact, Mia Levine (m.levine@sas.upenn.edu).

Materials availability—All reagents generated in this study are available upon request to the lead contact.

Data availability—The *mh* and *Top2* alleles from *D. simulans* have been deposited in GenBank and are publicly available as of the date of this publication. Accession numbers are listed in the key resources table. All other data reported in this paper will be shared by the lead contact upon request. This paper does not report original code. Any additional information required to reanalyze the data reported in this paper is available from the lead contact upon request.

EXPERIMENTAL MODEL AND SUBJECT DETAILS

We maintained *Drosophila melanogaster* stocks on standard cornmeal food at 24°C. Fly stocks used in this study are listed in the key resources table.

METHOD DETAILS

Population genetic and molecular evolution analyses—We conducted population genetic analysis of *mh* using multiple alleles from both *D. melanogaster* and *D. simulans*. We obtained nine *D. melanogaster mh* alleles (coordinates X:15472804-15475400, dmel r6.4) from lines collected in Lyon, France.[64] We amplified seven *D. simulans mh* alleles from lines collected in Nairobi, Kenya (Accession OL546458-OL546464).[65] Importantly, a duplication event occurred along the *D. simulans* lineage, resulting in a full-length copy of the *mh* ortholog, and a tandem partial duplicate.[66,67] To specifically amplify the full length *mh* ortholog, we designed primers that anneal to unique genomic sequence only (Table S3). We then prepared genomic DNA and conducted PCR amplification followed by Sanger sequencing using standard protocols. We aligned the sequences in Geneious using the Geneious Alignment algorithm with default settings (Geneious v11.1.5, Biomatters, Auckland, New Zealand) and confirmed alignment quality by eye. We performed a McDonald-Kreitman test[33] with the *D. melanogaster* and *D. simulans mh* coding sequences. We performed lineage-specific McDonald-Kreitman tests with the *D. yakuba mh* coding sequence as an outgroup to polarize mutations along the *D. melanogaster* and *D. simulans* linages.

Similarly, we conducted population genetic analysis of *Top2* using multiple alleles from both *D. melanogaster* and *D. simulans*. We obtained nine *D. melanogaster Top2* alleles (coordinates 2L:19447365-19453490, dmel r6.4) from lines collected in Lyon, France.[64] We amplified and Sanger sequenced seven *D. simulans Top2* alleles from lines collected in Nairobi, Kenya (Accession OL156853-OL156859).[65] As described above, we aligned the sequences in Geneious, confirmed alignment quality by eye, and performed a McDonald-Kreitman test.[33]

We calculated pairwise dN/dS between *D. melanogaster* and *D. simulans mh* alleles using a window size of 200bp (step size = 20bp) in the software package, DnaSP.[68] We reconstructed the ancestral *mh* sequence of *D. melanogaster* and *D. simulans* using the codeML package in PAML[69,70] and repeated this pairwise calculation between the extant *D. melanogaster* and *D. simulans mh* alleles and the reconstructed ancestral *mh* allele.

Fly stock construction

Constructing gene swaps: We used CRISPR/Cas9 to generate *D. melanogaster* flies that encode a transgenic *D. melanogaster* allele or a *D. simulans* allele of *mh*, integrated into the native location. We first generated a U6 promoter-driven guide RNA construct by cloning sgRNAs flanking the coding sequence of *mh* (5': GGATTGGCCCAGGATCAACA, 3': CGTGGAGAGCTTCTGCCGCG) into pBFv-U6.2 and pBFv-U6.2B backbones. We shuttled the 3' sgRNA into pBFv-U6.2 to create a dual sgRNA vector (University of Utah Mutagenesis Core). In parallel, we constructed homology directed repair (HDR) plasmids encoding one kilobase homology arms 5' and 3' of their respective guide RNAs. Between the homology arms we synthesized a codon-optimized (for *D. melanogaster*) *mh* coding sequence from either *D. melanogaster* or *D. simulans* (GenScript, Piscataway, NJ). We N-terminally tagged each sequence with 3xFLAG along with a linker sequence

(GGTGGTTCATCA). We injected the dual sgRNA vector and a single HDR plasmid into the Cas9-expressing line, *yw; nos-Cas9(II-attP40)* (BestGene Inc, Chino Hills, CA).

We crossed single males, injected as embryos, to FM7 (*X*-chromosome balancer) females. We screened F_1 females to identify positive transformants using forward primer 5'-AAGTGTCGCGCTATTTCACC-3' and reverse primer 5'-TCACCGTCATGGTCTTTGTAGTCCAT-3'. We then backcrossed the positive F_1 females to FM7 males and self-crossed the balanced F_2 progeny to generate lines homozygous for either *mh[mel]* or *mh[sim]* allele. To confirm that the introduced alleles encoded the expected sequence, we amplified the entire region from homozygous flies using primers that anneal outside of the homology arms (5'-AATGGATTTCGGCAAATGAG-3', 5'-GTCGTTGTAGGAGCCCATGT-3') and then sequenced across the entire region. We also designed primers that amplified the native *mh* locus (5'-GGCCCTGCTCATATCGTATC-3', 5'-AAGAACCTTACTGCGTGCAAC-3') to confirm that our final genotypes were true replacements. Finally, we confirmed that the transgenic alleles were introduced into only the endogenous *mh* location by performing inverse PCR using the APAgene GOLD Genome Walking Kit (Bio S&T, Inc, Montreal, Canada) following the manufacturer's instructions. The gene-specific primers for use in combination with the provided degenerate random tagging primers can be found in Table S3.

Constructing UAS-mh and UAS-Top2 lines: We used the *ΦC31* integrase-mediated transgenesis system to introduce into the same landing site *mh* from *D. melanogaster* or *D. simulans* downstream of an "upstream activating sequence" or "UAS"[71]. Using the HDR plasmids as a template (see above), we PCR-amplified the 3xFLA-Gtagged *mh* coding sequence (either *D. melanogaster* or *D. simulans)* using Phusion High-Fidelity DNA Polymerase (NEB, Ipswich, MA). We cloned the resulting PCR products into *NotI*/*XbaI* sites of the pUASp-attB vector (*Drosophila* Genomics Resource Center, Bloomington, IN). We confirmed the absence of PCR-introduced mutations in the cloned UASp-*mh[mel]* and UASp-*mh[sim]* alleles by direct Sanger sequencing of the constructs (Table S3). We introduced the constructs into *D. melanogaster yw; PBac[y$^+$-attP-9A]VK00018* flies, which have an attP transgene landing site at cytological position 75A10 on chromosome *3L* (BestGene Inc, Chino Hills, CA). We next made each transgene homozygous. To overexpress the transgenic alleles, we crossed these stocks to *Gal4::VP16-nos* (BDSC #64277), which drives germline expression of transgenes downstream of UAS.

Similarly, we used the *ΦC31* integrase-mediated transgenesis system to introduce *Top2* from *D. melanogaster* downstream of an UAS promoter.[71] We synthesized a codon-optimized, *D. melanogaster Top2* coding sequence (Twist, South San Francisco, CA). We N-terminally tagged each sequence with 3xHA along with a linker sequence (GGTGGTTCATCA). We introduced the constructs into *D. melanogaster yw; PBac[y$^+$-attP-9A]VK00018* flies (see above, BestGene Inc, Chino Hills, CA). We next constructed either *mh[mel]*; UASp-*Top2[mel]* or *mh[sim]*; UASp-*Top2[mel]* stocks using balancer chromosomes. To overexpress the transgenic *Top2* allele, we crossed either *mh[mel]*; UASp-*Top2[mel]* or *mh[sim]*; UASp-*Top2[mel]* males to either *mh[mel]*; *Gal4::VP16-nos* or *mh[sim]*; *Gal4::VP16-nos* females, respectively.

Zhr rescue stocks: To generate stocks that encode both the *X*-linked *mh*-transgene and the *X*-linked *359bp* satellite deletion (*Zhr*^{1}, BDSC #25140), we first generated trans-heterozygote females. We crossed these trans-heterozygote females to FM7 males and used PCR to assay individual recombinant male progeny for the presence of both the *mh* transgene and *Zhr*. We detected the *mh* transgenes with forward primer 5'-AAGTGTCGCGCTATTTCACC-3' and reverse primer 5'-TCACCGTCATGGTCTTTGTAGTCCAT-3'. To detect the *Zhr* mutation (*i.e.*, *359bp* satellite deletion), we used forward primer 5'-TATTCTTACATCTATGTGACC-3' and reverse primer 5'-GTTTTGAGCAGCTAATTACC-3'.[9] Performing a 10-cycle PCR at an annealing temperature of 52°C yields a band only in the presence of the 11Mb *359bp* satellite array (Figure 3B). We backcrossed males positive for both the *mh* transgene and *Zhr* mutation to FM7 females to generate a permanent stock.

Additional stocks: We generated heterozygous *mh[mel]*/*mh[sim]* females by crossing *mh[mel]* females to *mh[sim]* males.

We used a +/FM7; +/CyO stock to generate flies encoding both the *mh* transgene at the native locus (chromosome *X*) and the *Chk*$^{-/-}$ (*mnk*) mutation (chromosome *2*). The *mnk*^{l6} stock[41] was a gift from N. Phadnis.

To generate heterozygous *Top2* hypomorph females, we also used a +/FM7; +/CyO stock to construct flies encoding both the *mh* transgene at the native locus (chromosome *X*) and a heterozygous *Top2*$^{17-6}$/CyO mutation (chromosome *2*). The *Top2*$^{17-6}$ stock[72] was a gift from P. Geyer.

Immunoblotting—To assay 3xFLAG MH protein abundance in the ovary, we dissected 20 ovary pairs in 1X PBS and ground the material in RIPA buffer (Cell Signaling Technology, Danvers, MA), Protease Inhibitor Cocktail (Roche, Basel, Switzerland), and 2X PMSF (Cell Signaling Technology, Danvers, MA). To promote solubility, we incubated the lysate in benzonase (Sigma Aldrich, St. Louis, MO) for 1hr at 4C. We used 20μg of lysate and probed with 1:10,000 anti-FLAG (M2, Sigma Aldrich, St. Louis, MO) or 1:1000 anti-αTubulin (Developmental Studies Hybridoma Bank, Iowa City, IA) and 1:1000 anti-mouse HRP secondary antibodies (Kindle Biosciences, Greenwich, CT). We exposed blots with Kwikquant Western Blot detection kit and imaged with a Kwikquant imager (Kindle Biosciences, Greenwich, CT).

Fertility assays

Female fertility: To assay female fertility, we first aged virgin females 3–5 days. For each replicate vial, we crossed four virgin females to four *w*^{1118} males. We conducted crosses on molasses food at 24°C. UAS-Gal4 crosses were reared at 25°C. We flipped the parents onto new food every three days over the course of nine days and counted all progeny that emerged. No viability differences across assayed genotypes were noted.

Ovary size and mature egg counts: To determine the number of mature eggs and ovary size from focal genotypes, we first dissected ovary pairs in 1X PBS and imaged at 8X magnification with a Leica DFC7000 T camera. We quantified the area of each ovary pair

using the polygon tool in FIJI[73] to define the borders of the tissue. We then calculated the area (μm^2) within these boundaries using the "Measure" selection in FIJI. After imaging, we counted the number of eggs that contain elongated dorsal appendages (stages 13 and 14).

Immunofluorescence—We conducted immunofluorescence on ovaries following the protocol described in.[74] We stained ovaries with anti-FLAG (1:3000, M2, Sigma Aldrich, St. Louis, MO) and anti-γH2Av (1:1000, a gift from R. S. Hawley). We mounted ovaries with ProLong Gold Antifade Reagent with DAPI (Thermo Fisher Scientific, Waltham, MA). We imaged slides at 63X magnification on a Leica TCS SP8 Four Channel Spectral Confocal System. For each experiment, we used the same imaging parameters across genotypes.

We conducted immunofluorescence on embryos collected in a 0–70 minute window from *mh[mel]*, *mh[sim]*, or mh^1 females crossed to males homozygous for *P{gcid.EGFP.cid}III.2*[75], a gift from K. McKim. We followed the protocol described in[76] to fix and stain the embryos with anti-GFP (1:1000, Aves Labs, Tigard, OR). We mounted and imaged the embryos as described above.

Analysis of cytological data

Cell death quantification: To quantify the incidence of cell death, we mounted fixed whole ovaries (as described above) with ProLong Gold Antifade Reagent with DAPI (Thermo Fisher Scientific, Waltham, MA) and imaged at 63X magnification on a Leica TCS SP8 Four Channel Spectral Confocal System using the tile scanning and merging feature. We identified the number of ovarioles that contained egg chambers with >1 condensed, signal-saturated nurse cell nuclei. We then divided this number by the total number of ovarioles present in each ovary to determine the fraction of cell death incidence in *mh[mel]* and *mh[sim]* ovaries.

Immunofluorescence quantification: To quantify the average fluorescence of γH2Av in ovaries, we used the polygon tool in FIJI[73] to define the borders of a representative stage four egg chamber. We quantified the fluorescent signal intensity using the "Measure" tool in FIJI, which calculates the mean pixels within these boundaries. We normalized the fluorescent signal intensity of mh^1, *mh[mel]*, and *mh[sim]* to the mean intensity signal of the *mh[mel]*. Similarly, the fluorescent signal intensity of *mh[mel],Zhr* and *mh[sim],Zhr* was normalized to the mean intensity signal of *mh[mel],Zhr*. Finally, the fluorescent signal intensity of nos-Gal4-VP16 driven *mh[mel]*; UASp-*Top2[mel]* and *mh[sim]*; UASp-*Top2[mel]* was normalized to the mean intensity signal of nos-Gal4-VP16 driven *mh[mel]*; UASp-*Top2[mel]*.

QUANTIFICATION AND STATISTICAL ANALYSIS

We analyzed population genetic analyses using a χ^2 test and molecular evolution analyses using a Fisher's Exact test, otherwise we used t-tests. We carried out all statistical analyses using the R software (www.R-project.org).

Supplementary Material

Refer to Web version on PubMed Central for supplementary material.

ACKNOWLEDGEMENTS

We thank Isabella Farkas and Courtney Christopher for technical assistance, and the University of Utah Mutation Generation and Detection Core. We also thank the Levine Lab, M. Patel, N. Phadnis, A. Das, and D. Dudka for feedback on the manuscript and the Levine Lab, P. Geyer, H. Malik, R.S. Hawley, and M. Buszczak for discussions about the project. This work was supported by a Shurl and Kay Curci Foundation fellowship from the Life Sciences Research Foundation to C.L.B. and National Institutes of Health (NIH) NIGMS grant R35GM124684 to M.T.L.

REFERENCES

1. Cechova M, Harris RS, Tomaszkiewicz M, Arbeithuber B, Chiaromonte F, and Makova KD (2019). High satellite repeat turnover in great apes studied with short- and long-read technologies. Mol Biol Evol 36, 2415–2431. 10.1093/molbev/msz156.
2. Jagannathan M, Warsinger-Pepe N, Watase GJ, and Yamashita YM (2017). Comparative Analysis of Satellite DNA in the Drosophila melanogaster Species Complex. G3 (Bethesda) 7, 693–704. 10.1534/g3.116.035352. [PubMed: 28007840]
3. Kipling D, Ackford HE, Taylor BA, and Cooke HJ (1991). Mouse minor satellite DNA genetically maps to the centromere and is physically linked to the proximal telomere. Genomics 11, 235–241. 10.1016/0888-7543(91)90128-2. [PubMed: 1685135]
4. Round EK, Flowers SK, and Richards EJ (1997). Arabidopsis thaliana centromere regions: genetic map positions and repetitive DNA structure. Genome Res 7, 1045–1053. 10.1101/gr.7.11.1045. [PubMed: 9371740]
5. Rudd MK, and Willard HF (2004). Analysis of the centromeric regions of the human genome assembly. Trends Genet 20, 529–533. 10.1016/j.tig.2004.08.008. [PubMed: 15475110]
6. Mefford HC, and Trask BJ (2002). The complex structure and dynamic evolution of human subtelomeres. Nat Rev Genet 3, 91–102. 10.1038/nrg727. [PubMed: 11836503]
7. McKinley KL, and Cheeseman IM (2016). The molecular basis for centromere identity and function. Nat Rev Mol Cell Biol 17, 16–29. 10.1038/nrm.2015.5. [PubMed: 26601620]
8. Jagannathan M, Cummings R, and Yamashita YM (2018). A conserved function for pericentromeric satellite DNA. Elife 7. 10.7554/eLife.34122.
9. Rosic S, Kohler F, and Erhardt S (2014). Repetitive centromeric satellite RNA is essential for kinetochore formation and cell division. J Cell Biol 207, 335–349. 10.1083/jcb.201404097. [PubMed: 25365994]
10. Schoeftner S, and Blasco MA (2009). A 'higher order' of telomere regulation: telomere heterochromatin and telomeric RNAs. EMBO J 28, 2323–2336. 10.1038/emboj.2009.197. [PubMed: 19629032]
11. Henikoff S, Ahmad K, and Malik HS (2001). The centromere paradox: stable inheritance with rapidly evolving DNA. Science 293, 1098–1102. 10.1126/science.1062939. [PubMed: 11498581]
12. Lohe AR, Hilliker AJ, and Roberts PA (1993). Mapping simple repeated DNA sequences in heterochromatin of Drosophila melanogaster. Genetics 134, 1149–1174. [PubMed: 8375654]
13. Brutlag DL (1980). Molecular arrangement and evolution of heterochromatic DNA. Annu Rev Genet 14, 121–144. 10.1146/annurev.ge.14.120180.001005. [PubMed: 6260016]
14. de Lima LG, Hanlon SL, and Gerton JL (2020). Origins and Evolutionary Patterns of the 1.688 Satellite DNA Family in Drosophila Phylogeny. G3 (Bethesda) 10, 4129–4146. 10.1534/g3.120.401727. [PubMed: 32934018]
15. Tang X, Cao J, Zhang L, Huang Y, Zhang Q, and Rong YS (2017). Maternal Haploid, a Metalloprotease Enriched at the Largest Satellite Repeat and Essential for Genome Integrity in Drosophila Embryos. Genetics 206, 1829–1839. 10.1534/genetics.117.200949. [PubMed: 28615282]
16. Ferree PM, and Prasad S (2012). How can satellite DNA divergence cause reproductive isolation? Let us count the chromosomal ways. Genet Res Int 2012, 430136. 10.1155/2012/430136. [PubMed: 22567387]

17. Jagannathan M, and Yamashita YM (2021). Defective Satellite DNA Clustering into Chromocenters Underlies Hybrid Incompatibility in Drosophila. Mol Biol Evol 38, 4977–4986. 10.1093/molbev/msab221. [PubMed: 34302471]

18. Bayes JJ, and Malik HS (2009). Altered heterochromatin binding by a hybrid sterility protein in Drosophila sibling species. Science 326, 1538–1541. 10.1126/science.1181756. [PubMed: 19933102]

19. Kumon T, Ma J, Akins RB, Stefanik D, Nordgren CE, Kim J, Levine MT, and Lampson MA (2021). Parallel pathways for recruiting effector proteins determine centromere drive and suppression. Cell 184, 4904–4918 e4911. 10.1016/j.cell.2021.07.037. [PubMed: 34433012]

20. Maheshwari S, Tan EH, West A, Franklin FCH, Comai L, and Chan SWL (2015). Naturally occurring differences in CENH3 affect chromosome segregation in zygotic mitosis of hybrids. PLoS Genet 11, e1004970. 10.1371/journal.pgen.1004970. [PubMed: 25622028]

21. Ferree PM, and Barbash DA (2009). Species-specific heterochromatin prevents mitotic chromosome segregation to cause hybrid lethality in Drosophila. PLoS Biol 7, e1000234. 10.1371/journal.pbio.1000234. [PubMed: 19859525]

22. Gibeaux R, Acker R, Kitaoka M, Georgiou G, van Kruijsbergen I, Ford B, Marcotte EM, Nomura DK, Kwon T, Veenstra GJC, and Heald R (2018). Paternal chromosome loss and metabolic crisis contribute to hybrid inviability in Xenopus. Nature 553, 337–341. 10.1038/nature25188. [PubMed: 29320479]

23. Abad JP, Agudo M, Molina I, Losada A, Ripoll P, and Villasante A (2000). Pericentromeric regions containing 1.688 satellite DNA sequences show anti-kinetochore antibody staining in prometaphase chromosomes of Drosophila melanogaster. Mol Gen Genet 264, 371–377. 10.1007/s004380000331. [PubMed: 11129040]

24. Losada A, and Villasante A (1996). Autosomal location of a new subtype of 1.688 satellite DNA of Drosophila melanogaster. Chromosome Res 4, 372–383. 10.1007/BF02257273. [PubMed: 8871826]

25. Sproul JS, Khost DE, Eickbush DG, Negm S, Wei X, Wong I, and Larracuente AM (2020). Dynamic Evolution of Euchromatic Satellites on the X Chromosome in Drosophila melanogaster and the simulans Clade. Mol Biol Evol 37, 2241–2256. 10.1093/molbev/msaa078. [PubMed: 32191304]

26. Delabaere L, Orsi GA, Sapey-Triomphe L, Horard B, Couble P, and Loppin B (2014). The Spartan ortholog maternal haploid is required for paternal chromosome integrity in the Drosophila zygote. Curr Biol 24, 2281–2287. 10.1016/j.cub.2014.08.010. [PubMed: 25242033]

27. Svetec N, Cridland JM, Zhao L, and Begun DJ (2016). The Adaptive Significance of Natural Genetic Variation in the DNA Damage Response of Drosophila melanogaster. PLoS Genet 12, e1005869. 10.1371/journal.pgen.1005869. [PubMed: 26950216]

28. Loppin B, Berger F, and Couble P (2001). Paternal chromosome incorporation into the zygote nucleus is controlled by maternal haploid in Drosophila. Dev Biol 231, 383–396. 10.1006/dbio.2000.0152. [PubMed: 11237467]

29. Kihara S, Matsuzawa Y, Kubo M, Nozaki S, Funahashi T, Yamashita S, Sho N, and Tarui S (1989). Autoimmune hyperchylomicronemia. N Engl J Med 320, 1255–1259. 10.1056/NEJM198905113201906. [PubMed: 2785243]

30. Stingele J, Bellelli R, Alte F, Hewitt G, Sarek G, Maslen SL, Tsutakawa SE, Borg A, Kjaer S, Tainer JA, et al. (2016). Mechanism and Regulation of DNA-Protein Crosslink Repair by the DNA-Dependent Metalloprotease SPRTN. Mol Cell 64, 688–703. 10.1016/j.molcel.2016.09.031. [PubMed: 27871365]

31. Vaz B, Popovic M, Newman JA, Fielden J, Aitkenhead H, Halder S, Singh AN, Vendrell I, Fischer R, Torrecilla I, et al. (2016). Metalloprotease SPRTN/DVC1 Orchestrates Replication-Coupled DNA-Protein Crosslink Repair. Mol Cell 64, 704–719. 10.1016/j.molcel.2016.09.032. [PubMed: 27871366]

32. Weickert P, and Stingele J (2022). DNA-Protein Crosslinks and Their Resolution. Annu Rev Biochem. 10.1146/annurev-biochem-032620-105820.

33. McDonald JH, and Kreitman M (1991). Adaptive protein evolution at the Adh locus in Drosophila. Nature 351, 652–654. [PubMed: 1904993]

34. Garrigan D, Kingan SB, Geneva AJ, Andolfatto P, Clark AG, Thornton KR, and Presgraves DC (2012). Genome sequencing reveals complex speciation in the Drosophila simulans clade. Genome Res 22, 1499–1511. 10.1101/gr.130922.111. [PubMed: 22534282]
35. Kerr JF, Wyllie AH, and Currie AR (1972). Apoptosis: a basic biological phenomenon with wide-ranging implications in tissue kinetics. Br J Cancer 26, 239–257. 10.1038/bjc.1972.33. [PubMed: 4561027]
36. McCall K (2004). Eggs over easy: cell death in the Drosophila ovary. Dev Biol 274, 3–14. 10.1016/j.ydbio.2004.07.017. [PubMed: 15355784]
37. Roos WP, Thomas AD, and Kaina B (2016). DNA damage and the balance between survival and death in cancer biology. Nat Rev Cancer 16, 20–33. 10.1038/nrc.2015.2. [PubMed: 26678314]
38. Jang JK, Sherizen DE, Bhagat R, Manheim EA, and McKim KS (2003). Relationship of DNA double-strand breaks to synapsis in Drosophila. J Cell Sci 116, 3069–3077. 10.1242/jcs.00614. [PubMed: 12799415]
39. Madigan JP, Chotkowski HL, and Glaser RL (2002). DNA double-strand break-induced phosphorylation of Drosophila histone variant H2Av helps prevent radiation-induced apoptosis. Nucleic Acids Res 30, 3698–3705. 10.1093/nar/gkf496. [PubMed: 12202754]
40. Bakhrat A, Pritchett T, Peretz G, McCall K, and Abdu U (2010). Drosophila Chk2 and p53 proteins induce stage-specific cell death independently during oogenesis. Apoptosis 15, 1425–1434. 10.1007/s10495-010-0539-z. [PubMed: 20838898]
41. Brodsky MH, Weinert BT, Tsang G, Rong YS, McGinnis NM, Golic KG, Rio DC, and Rubin GM (2004). Drosophila melanogaster MNK/Chk2 and p53 regulate multiple DNA repair and apoptotic pathways following DNA damage. Mol Cell Biol 24, 1219–1231. 10.1128/MCB.24.3.1219-1231.2004. [PubMed: 14729967]
42. Sawamura K, Yamamoto MT, and Watanabe TK (1993). Hybrid lethal systems in the Drosophila melanogaster species complex. II. The Zygotic hybrid rescue (Zhr) gene of D. melanogaster. Genetics 133, 307–313. [PubMed: 8436277]
43. Dokshin GA, Davis GM, Sawle AD, Eldridge MD, Nicholls PK, Gourley TE, Romer KA, Molesworth LW, Tatnell HR, Ozturk AR, et al. (2020). GCNA Interacts with Spartan and Topoisomerase II to Regulate Genome Stability. Dev Cell 52, 53–68 e56. 10.1016/j.devcel.2019.11.006. [PubMed: 31839538]
44. Lopez-Mosqueda J, Maddi K, Prgomet S, Kalayil S, Marinovic-Terzic I, Terzic J, and Dikic I (2016). SPRTN is a mammalian DNA-binding metalloprotease that resolves DNA-protein crosslinks. Elife 5. 10.7554/eLife.21491.
45. Gale KC, and Osheroff N (1992). Intrinsic intermolecular DNA ligation activity of eukaryotic topoisomerase II. Potential roles in recombination. J Biol Chem 267, 12090–12097. [PubMed: 1318309]
46. Morimoto S, Tsuda M, Bunch H, Sasanuma H, Austin C, and Takeda S (2019). Type II DNA Topoisomerases Cause Spontaneous Double-Strand Breaks in Genomic DNA. Genes (Basel) 10. 10.3390/genes10110868.
47. Pommier Y, Sun Y, Huang SN, and Nitiss JL (2016). Roles of eukaryotic topoisomerases in transcription, replication and genomic stability. Nat Rev Mol Cell Biol 17, 703–721. 10.1038/nrm.2016.111. [PubMed: 27649880]
48. Kas E, and Laemmli UK (1992). In vivo topoisomerase II cleavage of the Drosophila histone and satellite III repeats: DNA sequence and structural characteristics. EMBO J 11, 705–716. [PubMed: 1311255]
49. Hughes SE, and Hawley RS (2014). Topoisomerase II is required for the proper separation of heterochromatic regions during Drosophila melanogaster female meiosis. PLoS Genet 10, e1004650. 10.1371/journal.pgen.1004650. [PubMed: 25340780]
50. Centore RC, Yazinski SA, Tse A, and Zou L (2012). Spartan/C1orf124, a reader of PCNA ubiquitylation and a regulator of UV-induced DNA damage response. Mol Cell 46, 625–635. 10.1016/j.molcel.2012.05.020. [PubMed: 22681887]
51. Reinking HK, Kang HS, Gotz MJ, Li HY, Kieser A, Zhao S, Acampora AC, Weickert P, Fessler E, Jae LT, et al. (2020). DNA Structure-Specific Cleavage of DNA-Protein Crosslinks by the SPRTN Protease. Mol Cell 80, 102–113 e106. 10.1016/j.molcel.2020.08.003. [PubMed: 32853547]

52. Zhao S, Kieser A, Li HY, Reinking HK, Weickert P, Euteneuer S, Yaneva D, Acampora AC, Gotz MJ, Feederle R, and Stingele J (2021). A ubiquitin switch controls autocatalytic inactivation of the DNA-protein crosslink repair protease SPRTN. Nucleic Acids Res 49, 902–915. 10.1093/nar/gkaa1224. [PubMed: 33348378]
53. Ferree PM, Gomez K, Rominger P, Howard D, Kornfeld H, and Barbash DA (2014). Heterochromatin position effects on circularized sex chromosomes cause filicidal embryonic lethality in Drosophila melanogaster. Genetics 196, 1001–1005. 10.1534/genetics.113.161075. [PubMed: 24478337]
54. Chmátal L, Gabriel SI, Mitsainas GP, Martínez-Vargas J, Ventura J, Searle JB, Schultz RM, and Lampson MA (2014). Centromere strength provides the cell biological basis for meiotic drive and karyotype evolution in mice. Current biology: CB 24, 2295–2300. 10.1016/j.cub.2014.08.017. [PubMed: 25242031]
55. Iwata-Otsubo A, Dawicki-McKenna JM, Akera T, Falk SJ, Chmátal L, Yang K, Sullivan BA, Schultz RM, Lampson MA, and Black BE (2017). Expanded Satellite Repeats Amplify a Discrete CENP-A Nucleosome Assembly Site on Chromosomes that Drive in Female Meiosis. Current biology: CB 27, 2365–2373.e2368. 10.1016/j.cub.2017.06.069. [PubMed: 28756949]
56. Malik HS, and Henikoff S (2001). Adaptive evolution of Cid, a centromere-specific histone in Drosophila. Genetics 157, 1293–1298. 10.1093/genetics/157.3.1293. [PubMed: 11238413]
57. Malik HS, and Henikoff S (2002). Conflict begets complexity: the evolution of centromeres. Curr Opin Genet Dev 12, 711–718. 10.1016/s0959-437x(02)00351-9. [PubMed: 12433586]
58. Vermaak D, Bayes JJ, and Malik HS (2009). A surrogate approach to study the evolution of noncoding DNA elements that organize eukaryotic genomes. J Hered 100, 624–636. 10.1093/jhered/esp063. [PubMed: 19635763]
59. Carracedo MC, Asenjo A, and Casares P (2000). Location of Shfr, a new gene that rescues hybrid female viability in crosses between Drosophila simulans females and D. melanogaster males. Heredity (Edinb) 84 (Pt 6), 630–638. 10.1046/j.1365-2540.2000.00658.x. [PubMed: 10886378]
60. Gerard PR, and Presgraves DC (2012). Abundant genetic variability in Drosophila simulans for hybrid female lethality in interspecific crosses to Drosophila melanogaster. Genet Res (Camb) 94, 1–7. 10.1017/S0016672312000031. [PubMed: 22353244]
61. Orr HA (1996). The unexpected recovery of hybrids in a Drosophila species cross: a genetic analysis. Genet Res 67, 11–18. 10.1017/s0016672300033437. [PubMed: 8919886]
62. Sawamura K, Taira T, and Watanabe TK (1993). Hybrid lethal systems in the Drosophila melanogaster species complex. I. The maternal hybrid rescue (mhr) gene of Drosophila simulans. Genetics 133, 299–305. [PubMed: 8436276]
63. Sawamura K, and Yamamoto MT (1993). Cytogenetical localization of Zygotic hybrid rescue (Zhr), a Drosophila melanogaster gene that rescues interspecific hybrids from embryonic lethality. Mol Gen Genet 239, 441–449. 10.1007/BF00276943. [PubMed: 8316215]
64. Pool JE, Corbett-Detig RB, Sugino RP, Stevens KA, Cardeno CM, Crepeau MW, Duchen P, Emerson JJ, Saelao P, Begun DJ, and Langley CH (2012). Population Genomics of sub-saharan Drosophila melanogaster: African diversity and non-African admixture. PLoS Genet 8, e1003080. 10.1371/journal.pgen.1003080. [PubMed: 23284287]
65. Rogers RL, Cridland JM, Shao L, Hu TT, Andolfatto P, and Thornton KR (2014). Landscape of standing variation for tandem duplications in Drosophila yakuba and Drosophila simulans. Mol Biol Evol 31, 1750–1766. 10.1093/molbev/msu124. [PubMed: 24710518]
66. Chakraborty M, Chang CH, Khost DE, Vedanayagam J, Adrion JR, Liao Y, Montooth KL, Meiklejohn CD, Larracuente AM, and Emerson JJ (2021). Evolution of genome structure in the Drosophila simulans species complex. Genome Res 31, 380–396. 10.1101/gr.263442.120. [PubMed: 33563718]
67. Castillo DM, Kean CM, McCormick B, Natesan S, and Barbash DA (2022). Testing the Drosophila maternal haploid gene for functional divergence and a role in hybrid incompatibility. bioRxiv. 10.1101/2022.03.23.485453.
68. Rozas J, Sanchez-DelBarrio JC, Messeguer X, and Rozas R (2003). DnaSP, DNA polymorphism analyses by the coalescent and other methods. Bioinformatics 19, 2496–2497. 10.1093/bioinformatics/btg359. [PubMed: 14668244]

69. Yang Z (1997). PAML: a program package for phylogenetic analysis by maximum likelihood. Comput Appl Biosci 13, 555–556. 10.1093/bioinformatics/13.5.555. [PubMed: 9367129]

70. Yang Z (2007). PAML 4: phylogenetic analysis by maximum likelihood. Mol Biol Evol 24, 1586–1591. msm088 [pii]10.1093/molbev/msm088. [PubMed: 17483113]

71. Venken KJ, He Y, Hoskins RA, and Bellen HJ (2006). P[acman]: a BAC transgenic platform for targeted insertion of large DNA fragments in D. melanogaster. Science 314, 1747–1751. 10.1126/science.1134426. [PubMed: 17138868]

72. Hohl AM, Thompson M, Soshnev AA, Wu J, Morris J, Hsieh TS, Wu CT, and Geyer PK (2012). Restoration of topoisomerase 2 function by complementation of defective monomers in Drosophila. Genetics 192, 843–856. 10.1534/genetics.112.144006. [PubMed: 22923380]

73. Schindelin J, Arganda-Carreras I, Frise E, Kaynig V, Longair M, Pietzsch T, Preibisch S, Rueden C, Saalfeld S, Schmid B, et al. (2012). Fiji: an open-source platform for biological-image analysis. Nat Methods 9, 676–682. 10.1038/nmeth.2019. [PubMed: 22743772]

74. McKim KS, Joyce EF, and Jang JK (2009). Cytological analysis of meiosis in fixed Drosophila ovaries. Methods Mol Biol 558, 197–216. 10.1007/978-1-60761-103-5_12. [PubMed: 19685326]

75. Schuh M, Lehner CF, and Heidmann S (2007). Incorporation of Drosophila CID/CENP-A and CENP-C into centromeres during early embryonic anaphase. Curr Biol 17, 237–243. 10.1016/j.cub.2006.11.051. [PubMed: 17222555]

76. Levine MT, Vander Wende HM, and Malik HS (2015). Mitotic fidelity requires transgenerational action of a testis-restricted HP1. Elife 4, e07378. 10.7554/eLife.07378. [PubMed: 26151671]

HIGHLIGHTS

- The *Drosophila* homolog of Spartan, Maternal Haploid (MH), evolves adaptively
- The *D. simulans* MH is toxic to oogenesis in its sister species, *D. melanogaster*
- *D. simulans* MH toxicity is triggered by a *D. melanogaster*-specific satellite array
- Overexpression of Top2 mitigates this *D. melanogaster*-*D. simulans* incompatibility

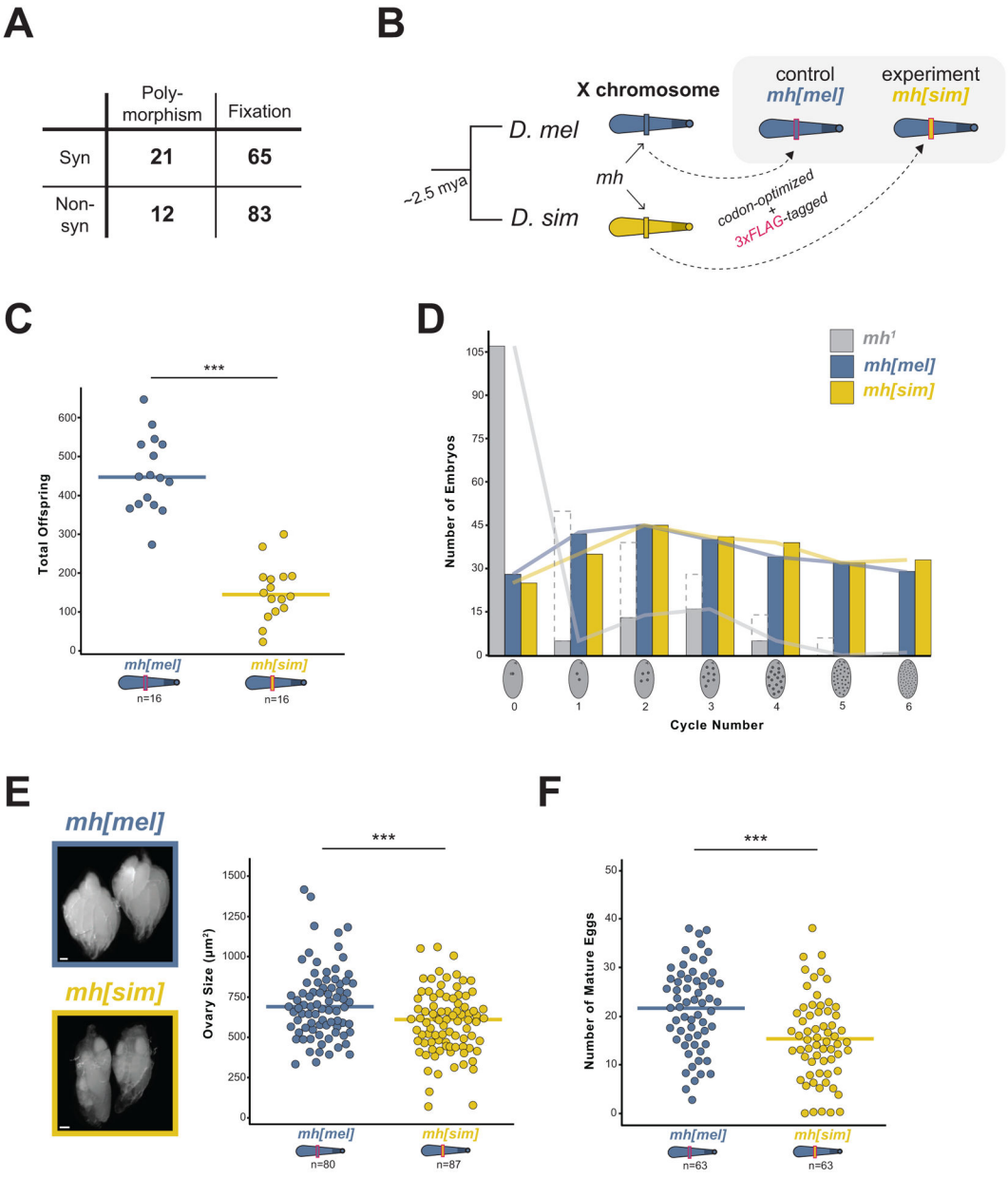

Figure 1. MH evolves adaptively to preserve female fertility.

(A) Counts of synonymous and nonsynonymous polymorphic and fixed sites within and between *D. melanogaster* and *D. simulans;* χ^2 test, p = 0.04. (B) Swap strategy: the *D. melanogaster* ("*mel*", blue) or *D. simulans* ("*sim*," yellow) *mh* coding sequence, codon-optimized for *D. melanogaster* and 3xFLAG-tagged, replaced the native *mh* gene on the *X* chromosome. (C) Total offspring from *mh[mel]* or *mh[sim]* females crossed to wildtype (w^{1118}) males. (D) Frequency distribution of embryos at increasing mitotic cycle numbers collected for 70 minutes from mh^1, *mh[mel]*, and *mh[sim]* females. Dashed bars from mh^1 females correspond to embryos undergoing mitotic catastrophe likely triggered at the first mitosis. Solid gray bars representing mh^1-derived embryos greater than cycle 0 are presumed maternal haploid. (E) Representative images and ovary size estimates from

mh[mel] and *mh[sim]* females. (F) Number of mature eggs per ovary pair from *mh[mel]* and *mh[sim]* females. (*t*-test: "***" = $p < 0.001$, scale bar = 100μm)

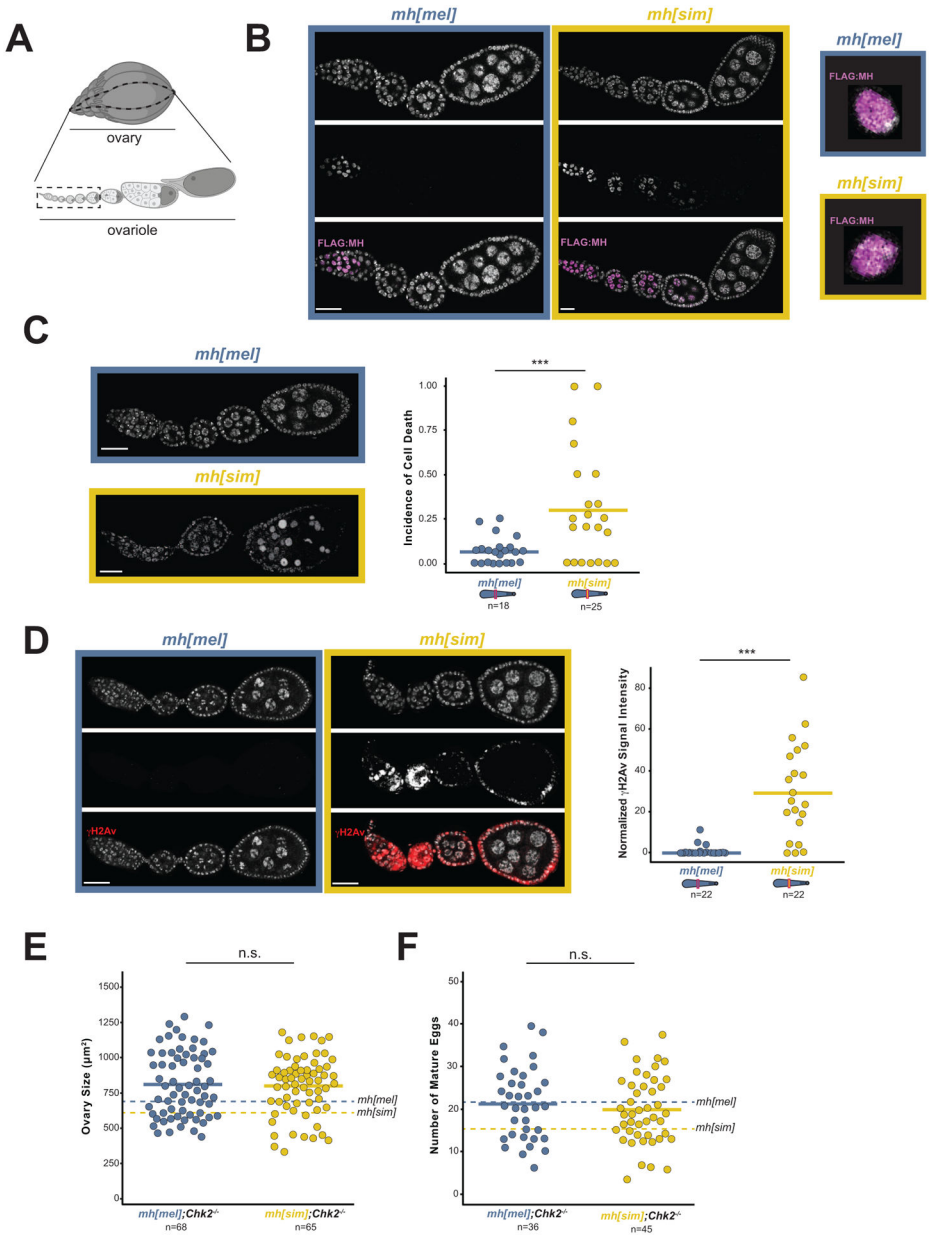

Figure 2. MH[sim] poisons oogenesis through a DNA damage pathway.

(A) Diagram of a Drosophila ovary (above) and a single ovariole (below) with the germline stem cells in the germarium at the anterior (left) position and the mature eggs at the posterior position (right). The dashed box shows the developmental stages shown in images 2B-2D (Created using BioRender.com). (B) *mh[mel]* and *mh[sim]* ovaries stained with anti-FLAG to visualize MH localization (left). Merged images of single nuclei from the germarium (*) show no MH foci on the DNA (right). (C) Incidence of cell death captured by the fraction of ovarioles with condensed nuclei (arrowheads) in *mh[mel]* and *mh[sim]* ovaries. (D) γH2Av signal in *mh[mel]* and *mh[sim]* ovaries and the quantification of normalized fluorescent signal intensity. Note that the expected γH2Av-positive cells in the germarium in *mh[mel]* are absent under the imaging parameters used but are indeed present, see Figure S3A. (E)

Ovary size estimates from *mh[mel]; Chk2*$^{-/-}$ and *mh[sim]; Chk2*$^{-/-}$ females. (F) Number of mature eggs per ovary pair from *mh[mel]; Chk2*$^{-/-}$ and *mh[sim]; Chk2*$^{-/-}$ females. In panels E and F, dotted lines correspond to *mh[mel]* and *mh[sim]* averages reported in Figure 1E and 1F, respectively. (*t*-test: "***" = $p < 0.001$, "n.s." $p > 0.05$, scale bar = 25μm)

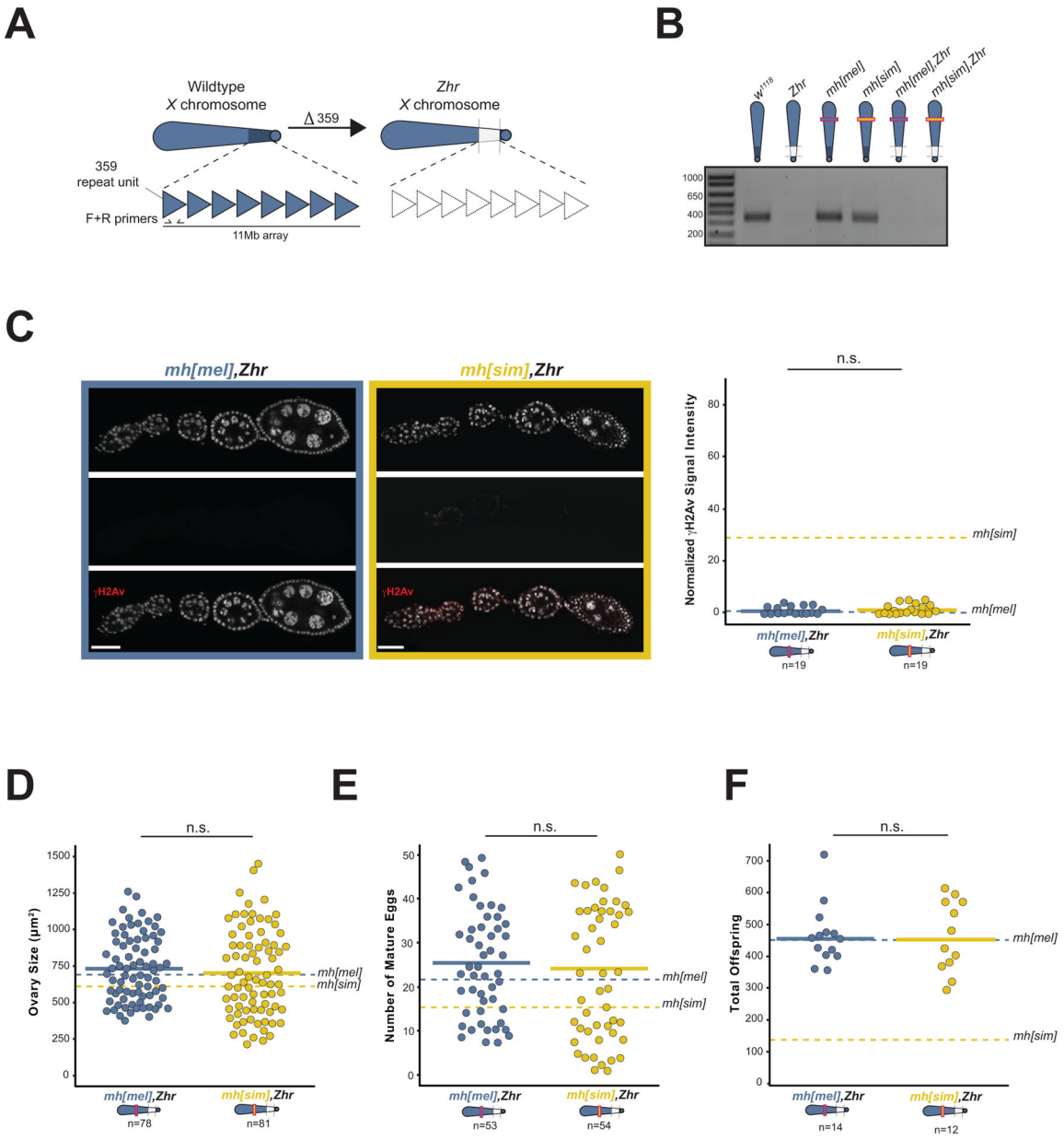

Figure 3. The *359bp* satellite deletion rescues *mh[sim]* genome integrity and fertility.

(A) The ***Z****hr X* chromosome lacks the 11Mb pericentromeric *359bp* satellite array. (B) A 10-cycle PCR distinguishes between wildtype *359bp* copy number and the *359bp* deletion (*Zhr*) and validates the recombined *mh[mel],Zhr* and recombined *mh[sim],Zhr X* chromosomes. (C) γH2Av signal in *mh[mel],Zhr* and *mh[sim],Zhr* ovaries and the quantification of normalized fluorescent signal intensity. Dotted lines correspond to *mh[mel]* and *mh[sim]* averages reported in Figure 2D. (D) Ovary size of *mh[mel],Zhr* and *mh[sim],Zhr* females. (E) Number of mature eggs per ovary pair from *mh[mel],Zhr* and *mh[sim],Zhr* females. (F) Progeny counts from *mh[mel],Zhr* and *mh[sim],Zhr* females crossed to wildtype (w^{1118}) males. In panels D, E, and F, dotted lines correspond to *mh[mel]* and *mh[sim]* averages reported in Figure 1E, 1F, and 1C, respectively. (*t*-test: "n.s." $p > 0.05$, scale bar = 25μm)

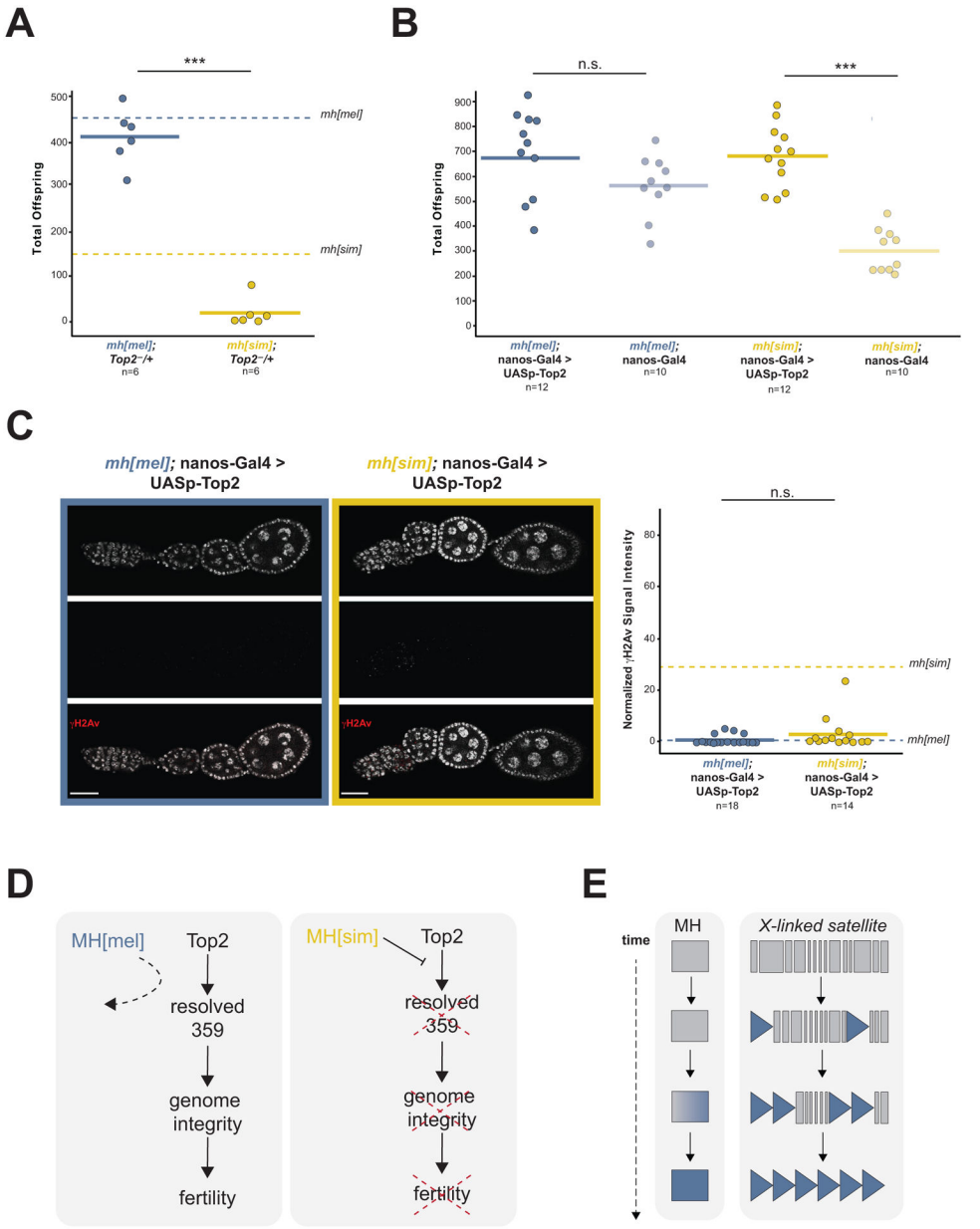

Figure 4. MH[sim] may interfere with Top2 processing of *359bp* entanglements.

(A) Progeny counts from *mh[mel]; Top2*$^{-}$*/+* and *mh[sim]; Top2*$^{-}$*/+* females crossed to wildtype (*w*^{1118}) males. Dotted lines correspond to *mh[mel]* and *mh[sim]* averages reported in Figure 1C. (B) Progeny counts from nos-Gal4-VP16 (female germline GAL4) driven *mh[mel];* UASp-*Top2* or *mh[sim];* UASp-*Top2* females crossed to wildtype (*w*^{1118}) males. (C) γH2Av signal from ovaries of nos-Gal4-VP16 driven *mh[mel];* UASp-*Top2* or *mh[sim];* UASp-*Top2* females and quantification of normalized fluorescent signal intensity. Dotted lines correspond to *mh[mel]* and *mh[sim]* averages reported in Figure 2D. (D) Model of MH[sim] interference with Top2 processing of *359bp* entanglements. These entanglements threaten genome integrity and ultimately, fertility. MH[mel], in contrast, has no measurable function in the ovaries, suggesting that it avoids interfering with *359bp* processing by Top2.

(E) Model of MH evolution tracking *359bp* satellite proliferation. (*t*-test: "***" = $p < 0.001$, "n.s." $p > 0.05$, scale bar = 25μm)

Key resources table

REAGENT or RESOURCE	SOURCE	IDENTIFIER
Antibodies		
Mouse Monoclonal anti-FLAG M2	Sigma-Aldrich	Cat#F3165
Mouse Monoclonal 12G10 anti-αTubulin	Developmental Studies Hybridoma Bank	Cat#12G10 anti-alpha-tubulin, RRID:AB_1157911
Mouse Monocolonal anti-Histone 2A Gamma Variant, Phosphorylated	Developmental Studies Hybridoma Bank	Cat#UNC93–5.2.1, RRID:AB_261807
Chicken Polyconal anti-Green Fluorescent Protein	Aves Labs	Cat# GFP-1010, RRID:AB_230731
Chemicals, peptides, and recombinant proteins		
Phusion High-Fidelity DNA Polymerase	NEB	Cat#M0530
RIPA buffer	Cell Signaling Technology	Cat#9806
Protease Inhibitor Cocktail	Roche	Cat#11873580001
PMSF	Cell Signaling Technology	Cat#8553
Benzonase	Sigma-Aldrich	Cat#E1014
ProLong Gold Antifade Mountant with DAPI	ThermoFisher Scientific	Cat#P36931
Critical commercial assays		
APAgene GOLD Genome Walking Kit	Bio S&T, Inc	BT901-RT
Kwikquant Western Blot Detection Kit	Kindle Biosciences	Cat#R1004
Deposited data		
mh alleles from *D. simulans*	This manuscript	OL546458..64
Top2 alleles from *D. simulans*	This manuscript	OL156853..59
Experimental models: Organisms/strains		
yw; nos-Cas9(II-attP40)	Best Gene, Inc	N/A
yw; PBac[y^{+}-attP-9A]VK00018	Bloomington Drosophila Stock Center	BDSC:9736
Gal4::VP16-nos	Bloomington Drosophila Stock Center	BDSC:64277
Zhr^{1}	Bloomington Drosophila Stock Center	BDSC:25140
mnk^{l6}	N. Phadnis	N/A
Top2$^{17-6}$	P. Geyer	N/A
w^{1118}	MTL laboratory	N/A
mh^{1}	Bloomington Drosophila Stock Center	BDSC:7130
P{gcid.EGFP.cidIII}.2	K. McKim, *Schuh et al.*[75]	N/A
Oligonucleotides		
Primers to amplify and sequence *mh* alleles from *D. simulans*, see Table S3	This manuscript	N/A
Primers to screen *mh* CRISPR transformants, see Table S3	This manuscript	N/A
Primers to screen for PCR-introduced mutations in the cloned *mh* UAS constructs, see Table S3	This manuscript	N/A
Primers to detect native *mh* locus, see Table S3	This manuscript	N/A

REAGENT or RESOURCE	SOURCE	IDENTIFIER
Primers to screen for *359-bp* deletion (*Zhr*), see Table S3	Rosic *et al.*[9]	N/A
Primers for Genome Walking, see Table S3	This manuscript	N/A
Primers to amplify and sequence *Top2* alleles from *D. simulans*, see Table S3	This manuscript	N/A
Recombinant DNA		
Plasmid: pBFv-U6.2	Addgene	Addgene#138400
Plasmid: pBFv-U6.2B	Addgene	Addgene#138401
Plasmid: 3xFLAG:*mh[mel]* and 3xFLAG:*mh[sim]* HDR plasmids	This manuscript	N/A
Plasmid: pUASp-attB	Drosophila Genomics Resource Center	DGRC#1358
Software and algorithms		
Geneious v 11.1.5	Biomatters	https://www.geneious.com/
FIJI	ImageJ2	https://imagej.net/software/fiji/